

Feedback-optimized operations with linear ion crystals

J. F. Eble,¹ S. Ulm,^{1,*} P. Zahariev,² F. Schmidt-Kaler,¹ and K. Singer¹

¹*Institut für Quanteninformationsverarbeitung, Universität Ulm, Albert-Einstein-Allee 11, D-89069 Ulm, Germany*

²*Institute of Solid State Physics, Bulgarian Academy of Science, Tzarigradsko Chaussee Boulevard 72, 1784 Sofia, Bulgaria*

*Corresponding author: stefan.ulm@uni-ulm.de

Received December 2, 2009; revised February 28, 2010; accepted March 6, 2010;
posted March 19, 2010 (Doc. ID 120831); published April 27, 2010

We report transport operations with linear crystals of $^{40}\text{Ca}^+$ ions performed by applying complex electric time-dependent potentials. For their control we use the information obtained from the ions' fluorescence. We demonstrate that by means of this feedback technique, we can transport a predefined number of ions and also split and unify ion crystals. The feedback control allows for a robust scheme, compensating for experimental errors, as it does not rely on a precisely known electrical modeling of the electric potentials in the ion trap beforehand. Our method allows us to generate a self-learning voltage ramp for the required process. With an experimental demonstration of a transport with more than 99.8% success probability, this technique may facilitate the operation of a future ion-based quantum processor. © 2010 Optical Society of America

OCIS codes: 020.1335, 100.3008, 270.5585.

1. INTRODUCTION

Single trapped ions are promising candidates for the realization of quantum information processing. Quantum computing with as many as eight ions already has been successfully demonstrated [1]. However, the complexity of the control of an ion crystal in an electrostatic potential rapidly increases with the number of participating ions. Therefore, it is preferable to divide an ion trap into processing and storage regions where different actions like ion loading or ion addressing with specific laser pulses are performed [2,3]. A highly reliable method for the shuttling of ions in microsegmented traps [4] is essential.

In current schemes, a predefined amount of ions has been shuttled between different areas of the trap, as required for a future quantum processor. The transport of single ions in a linear Paul trap and the symmetric separation of a two-ion crystal has been reported. A success probability exceeding 95% has been shown [5]. The latest research in ion transport demonstrates shuttling through an X junction [6]. Even optimal control theory has been used to evaluate best time-dependent potential alterations for fast nonadiabatic transport of ions through the trap [7], and extended calculations [8] are necessary to obtain proper results. However, the theoretical outcome of optimal control cannot be directly transferred to the experiment because the calculated potentials are derived from a trap model that does not necessarily exactly match the real experimental situation. Fabrication imperfections cause aberrations between the real trap geometry and the theoretical model. Patch charges on the surface of the trap electrodes may even worsen the situation because voltage changes of the order of 10 μV can lead to a completely different potential shape during critical situations, such as splitting operations during which a very shallow potential occurs. Similar problems may also occur

for neutral atoms, where a deterministic transport has been accomplished by controlling the motion of a standing-wave in a dipole trap [9], and an optimal control scheme was proposed to improve the fidelity in a collisional gate [10].

In our approach for controlling a multiple-ion crystal our aim is to automate most of the operational building blocks. We are using the information from the observation of the ion crystal to feedback control the trap potentials in a robust way. Our method can adapt to geometric imperfections, patch potentials, and voltage supply drifts if inserted as a calibration operation between experimental runs. Thus we have realized the transport of ions over 1 mm, the separation of single ions from a linear crystal, and the rejoining of crystals in a realistic trap without any prior knowledge of the potentials. Potential changes are sensed from ion locations and compensated automatically by the feedback system. Feedback techniques are commonly used with ion traps in situations such as feedback cooling of ions [11], as well as error correction [12] or teleportation [13,14]; in all those cases the next steps of operation depend on the information read out from the quantum system itself.

Photographic recording of a single ion was first realized in a radio frequency trap [15]. A sudden step in fluorescence is associated with the arrival and departure of individual trapped atoms. Similar discrete levels of fluorescence are also observed with single neutral atoms in a magneto-optical or dipole trap [16,17]. For single fluorescing neutral atoms in a magneto-optical or dipole trap, the discrete levels of fluorescence prove the trapping of zero or one atom [18]. Sensitive EMCCD (electron-multiplying charge-coupled device) cameras allow for space- and time-resolved observation and imaging of single fluorescing atoms or ions, which is essential for the work presented.

The paper is organized as follows: a description of the experimental setup as well as a short overview of the potential simulation is given in Section 2. Automatic loading and detection of a certain number of ions is demonstrated in Section 3. In Section 4, we explain our method for estimating the position of trapped ions. Positioning ions via feedback control and displacing them to a given position is shown in Section 5. We continue with the automatic separation of an ion crystal with an adaptive gain control and the splitting into separated potentials in Section 6. We conclude with a discussion of future applications and improvements of our method.

2. EXPERIMENTAL SETUP

The segmented linear Paul trap consists of four blades, each featuring a total of 15 independent dc segments [7]. As the segments in the trap region are the most important, the middle electrode where the ion crystal is initially trapped is labeled as segment M, whereas the segments to the left and to the right of the visual focus of the camera are labeled with increasing indices as {L1, L2,...} and {R1, R2,...}, respectively. The blades are assembled in a X-shaped manner. Each blade has an additional electrode on the edge facing the ion. Two of these opposing segments are connected to the rf supply, whereas the other two opposing segments are used for compensation (see Fig. 1).

The blade material is polyimide [19] with 18 μm copper plating on both sides; the strip lines are produced by using standard lithography and etching techniques. The blades are electropolished to decrease surface roughness; additionally, they are coated with gold to become a chemically inactive surface. The trap region we use consists of eight 700 μm wide segments separated by 100 μm insulator. The radial distance between two trap electrodes equals 2 mm. The trap is housed in a stainless steel vacuum chamber. The base pressure is below 10^{-12} hPa. The rf peak-peak voltage for the radial confinement equals $U_{\text{rf}}=400$ V_{pp} at a trap drive frequency of $\Omega/2\pi=13.4$ MHz, resulting in a radial potential with trapping frequency $\omega_{\text{rad}}/2\pi=431.65$ kHz, exceeding the axial confinement. This ensures that as many as ten ions can be arranged in a linear configuration. Fast dc voltage control for each trap electrode is accomplished via a personal computer by an array of digital-analog converters [20]. Their voltages range from -10 to 10 V with a resolution of

16 bits, resulting in a smallest step size of 300 μV . This resolution is adequate because distant electrodes can be used for high-resolution potential changes. Each voltage supply is low-pass filtered (cutoff frequency 390 Hz).

The ionization of ^{40}Ca atoms is accomplished with a two-photon process by laser light near 423 nm and 374 nm [21]. For optical cooling and excitation, we illuminate the ion with laser light near 397, 866, and 854 nm and observe continuous fluorescence. The detection system consists of a specifically designed lens with NA = 0.30, which is placed 61 mm from the trap center at an angle perpendicular to the trap axis, and an EMCCD camera [22] featuring 1004×1002 pixels with a size of $8 \mu\text{m} \times 8 \mu\text{m}$. A distance calibration with higher accuracy is obtained by measuring the axial frequency and the distance of two ions. By applying a rf voltage to segment L6, an ion oscillation in the axial direction is stimulated. The currently chosen potential yields an axial frequency of $\omega_{\text{ax}}/2\pi=226.3 \pm 0.2$ kHz, whereas a distant unfiltered electrode is utilized for oscillation excitation. The ions' interdistance on the camera picture is 21.85 ± 0.02 pixels. This results in a distance calibration of $0.6908 \pm 0.0005 \mu\text{m}/\text{pixel}$ [23]. The axial potential distribution may be simulated with the boundary element method by using a 3D model of the trap [24]. With given voltages on the individual segments, we extract the resulting axial potential.

3. AUTOMATIC ION LOADING AND AMOUNT DETERMINATION

For the determination of the amount of ions in the trap, images are taken by the EMCCD camera. These images contain the count distribution $C(h, v)$, with $\{h, v\}$ denoting the pixel position in horizontal and vertical directions, respectively. In the following, we describe a fast, real-time image analysis used to determine the number of ions and their positions. Compared with a standard offline 2D Gaussian fit, our real-time method allows for a fast feedback, with a slightly reduced position accuracy. Our algorithm is only a first approach and does not take into account asymmetric imaging distortions; in future experiments fast 1D Gaussian fits will be tested for precise ion position determination.

As the ion crystal only illuminates a small area on the EMCCD chip, we choose a region of interest of 60×250 pixels from the full image of the camera. We sum the EMCCD counts over each column, $C(h)=\sum_v C(h, v)$ [see Fig. 2(b)]. To get the number of ions, we compute the maximum of $C(h)$ and introduce a threshold parameter, which is varied between the average background noise B and C_{max} . With this threshold parameter, it is possible to discriminate between closely spaced ions even if the fluorescence is overlapping and between unequally fluorescent ions stemming from the Gaussian profiled exciting laser beam. The background noise originates from stray light that is reflected back from the trap and readout noise of the EMCCD. In the next step, we set each value in $C(h)$ that is below the threshold parameter to zero and get the array $\tilde{C}(h)$ [see Fig. 2(c)] containing regions with counts and regions with zeros, yielding the number of ions in the crystal. While continuously analyzing the current

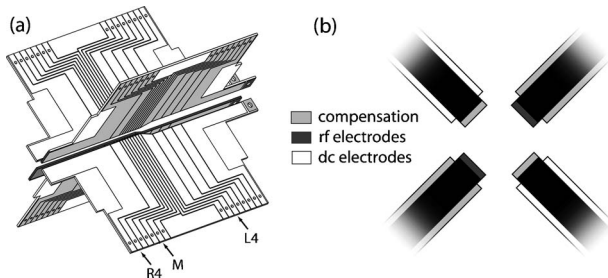


Fig. 1. (a) Sketch of the segmented linear Paul trap with dc electrodes depicted in white and rf-electrodes in dark gray. Compensation electrodes are light gray. (b) Front view, showing that the rf electrodes cover only two front faces of the blades. The other two are utilized as compensation electrodes.

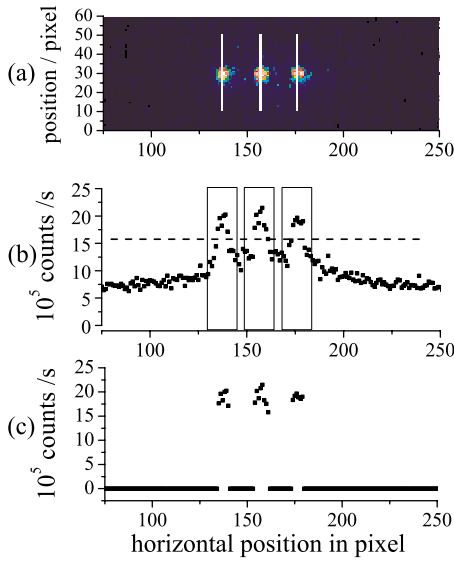


Fig. 2. (Color online) Ion position determination: (a) camera image of fluorescing ions with vertical markers to indicate the ion positions. (b) Vertically summed counts $C(h)$ with threshold parameter, here 60%, as the dashed line, and boxes wherein precise ion location takes place. (c) Vertically summed counts $\tilde{C}(h)$ (values below threshold are set to zero) for number and coarse location determination of the ions.

camera picture, we load a predefined number of ions by opening and blocking the ionization light. The loading efficiency for each desired number between 1 and 10 ions is 100% if the loading rate and the potential shape are chosen properly.

4. ION POSITION DETERMINATION

For each ion, we determine the position h_{ion} by utilizing the following method:

$$h_{\text{ion}} = \frac{\sum_h h(C(h) - B)}{\sum_h (C(h) - B)}, \quad (1)$$

where $(C(h) - B)$ are pixel counts corrected by the background noise level and h is chosen such that it covers the range of one ion only. On a recorded data set of 3000 images with an exposure time of $\tau = 100$ ms, we made a comparison between our method for determining the position and the 2D Gaussian fit. Our method reached an accuracy of 170 nm, and the Gaussian fit yielded a 100 nm accuracy. Our method is preferable in situations where fast reaction time and robustness to variations of $C(h)$ is crucial. As expected, the accuracy increases with $\sqrt{\tau}$.

In the experiment, see Fig. 3, we apply the location algorithm to an ion crystal consisting of nine ions; for a

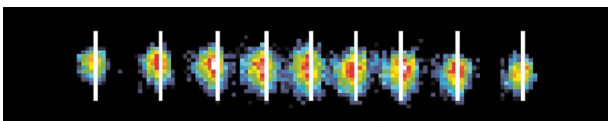


Fig. 3. (Color online) Ion crystal with automatically determined equilibrium positions. The exposure time τ was set to 150 ms.

proper linear arrangement the rf amplitude is increased to $650 V_{\text{pp}}$. Assuming a harmonic potential in the axial direction, the determined locations agree within about one fifth of one pixel with theoretical values [23]. The automatically determined ion locations relative to the centered ion are (values in micrometers)

experimental: $-36.0, -25.0, -15.9, -7.6, 0, 8.1, 16.4, 25.3, 35.8$

theoretical:

$-35.78, -25.22, -16.28, -8.00, 0, 8.00, 16.28, 25.22, 35.78$

5. FEEDBACK ION POSITION REGULATION

To keep a single ion or an ion crystal fixed at one position in the presence of external disturbances, we performed feedback control. The trapping potential is created by a negative voltage on segment M and positive voltages on segment L1 and R1. We used a camera exposure time of 25 ms (maximum available gain). The feedback control was implemented by a digital proportional and integral (PI) controller, which is fed with the position information x_{act} from the ion position determination algorithm described above. Comparing the actual value with a target value x_{aim} , the PI control regulates the ion position in axial direction by changing the voltage $V_{L1} = V_{L1}^{\text{old}} - \Delta V_{L1}$ of segment L1. The PI-controlled voltage change ΔV_{L1} is calculated as

$$\Delta V_{L1} = P \cdot (x_{\text{aim}} - x_{\text{act}}) + I \cdot \sum_k (x_{\text{aim}} - x_k), \quad (2)$$

where the integral term is updated in each step k . A term pertaining to the derivative does not improve the regulation and is therefore omitted. In the test routine, the ion was regulated alternately between the initial ion position and a position shifted 60 pixels to the left, which corresponds to a distance of $41.4 \mu\text{m}$. The optimal PI gain is found for $P = 7$ mV/pixel and $I = 1$ mV/pixel, but the regulation still works if these optimal values are multiplied by a factor of 0.5 to 2. Please note that the optimal gain depends on the trapping potential; see Section 6.

In Fig. 4 the position of the ion is shown during the regulation at two distinct locations A and B as a function of the time. From a large number of transports, we determine a success probability of 99.8% where the new position is achieved within a time span of 600 ms. A successful transport is assumed if the ion is transported to the wanted position without loss. Included in the success probability is the normal loss of ions due to background gas collisions.

Interestingly, the required control voltage V_{L1} does barely show any variation for the consecutive transports; see also Fig. 5. The algorithm has learned the way to transport an ion without making any assumptions about the potentials generated by the electrodes.

The PI regulation adapts the voltage ramp only if external disturbances occur. Due to the robustness of our detection algorithm, which allows even the localization of blurred ions to some degree, the PI controller can handle strong disturbances of the trapping potential. It is limited only by the extension of the laser beam diameter with a

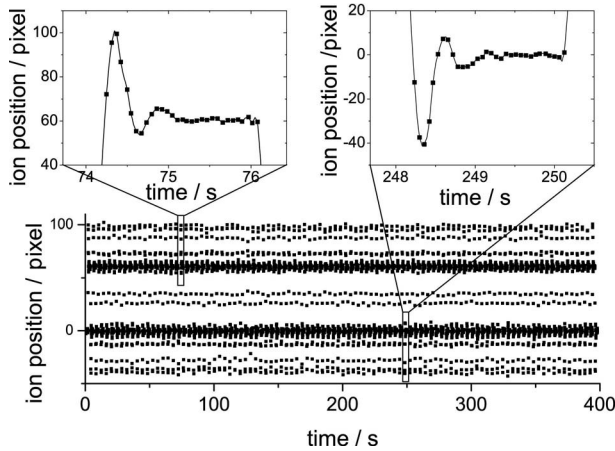


Fig. 4. Feedback-regulated ion positions as a function of time, consisting of 100 consecutively executed forth-and-back regulations over 60 pixels. Left insert, enlargement of a single regulation process for moving the ion from position A to B in an abrupt manner; right insert, regulation for transporting the ion from B to A. Here, the regulation between A and B is accomplished within 600 ms.

FWHM of $76 \mu\text{m}$, as we need a sufficient number of fluorescence photons to gain an adequate signal-to-noise ratio for the PI regulator. A typical application for this kind of PI control may be a repetitive ion position adjustment during long-term ion trap experiments, where patch charges or other disturbances cause an axial ion drift.

6. AUTOMATIC SPLITTING OF AN ION CRYSTAL

The separation is performed in two different ways: During a symmetric separation, the ion crystal is divided such that two equal parts move equally far apart from the initial position into well-separated axial potential wells. Typically, the initial position of the crystal is exactly above one trap control segment, whose voltage is ramped down [5]. In the case of an asymmetric splitting, one or more ions may be kept at fixed positions, while another

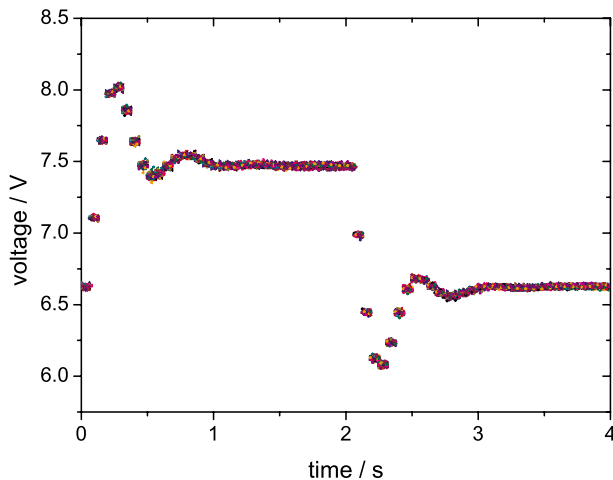


Fig. 5. (Color online) Control voltage alterations on segment L1 for 100 cycles with different colors for each loop. The repetitions, lying upon each other, indicate similar reactions of the system.

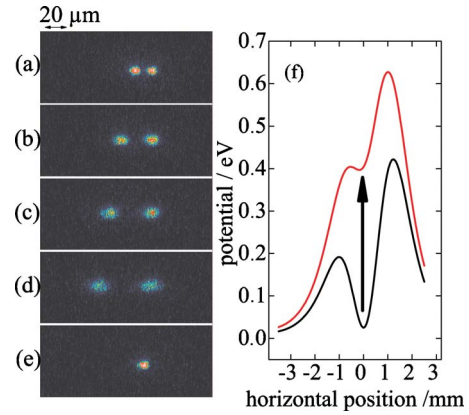


Fig. 6. (Color online) Automatic asymmetric splitting of a two-ion crystal. Camera pictures of fluorescent ions (a) before, (b)–(d) during, and (e) after the splitting process. (b)–(d) are taken after decreasing the potential depth and moving the left-hand ion. (f) Simulated potentials, showing the alteration of the potential during splitting process. Starting with a deep potential at the beginning of the splitting process, the voltages are changed in such a way that one ends with a shallow potential briefly before the crystal splits. In (e), only the right-hand ion stays in the trapping potential. Here, the potential is set to its initial values, such that the ion location is precisely in the middle of the two ions depicted in (a).

part of the crystal is split off. Here, the position of the ion crystal is not limited to be exactly above a specific segment.

To split a two-ion crystal in the asymmetric mode, we start with a deep axial trapping potential created by a negative voltage on segment M and positive voltages on segment L1 and segment R1, respectively (see Fig. 6). This configuration results in a localization of the ion crystal above segment M. We reduce the potential depth by lowering the voltage supplied to segment M and controlling the axial position with segment L1, while segment R1 is held at a fixed value. The lowering of the potential is performed in such a way that the inter-ion distance increases linearly. With the relation between the minimal ion–ion distance in a harmonic potential and the axial frequency $\Delta x \propto \omega_{\text{ax}}^{-2/3}$ [23], and by using the relation $\omega_{\text{ax}} \propto V_{\text{ax}}^{1/2}$ between the axial trapping frequency ω_{ax} and the axial confinement voltage V_{ax} , we find that $\Delta x \propto V_{\text{ax}}^{-1/3}$. In a segmented linear Paul trap with ions above segment M the axial voltage is given by $V_{\text{ax}} = V_{\text{L1/R1}} - V_{\text{M}}$, whereas the lower lateral voltage is taken. A linear increase of the ion–ion distance can be described by $mt + \Delta x_0$, where Δx_0 denotes the initial distance and m the voltage alteration velocity. The voltage alteration on segment M for decreasing the potential depth is then given by

$$V_{\text{M}} = V_{\text{L1/R1}} - \frac{A}{(mt + \Delta x_0)^3}, \quad (3)$$

where the constant A is deduced from $V_{\text{M}}(t=0)$. During the decrease of the trap depth, the minimum of the potential is also shifted, but this is balanced with control segment L1 via the PI control. However, the PI gain parameters need to be dynamically adapted for this task, in contrast to the transport of ions in a potential with fixed axial trapping frequency. With a change of the axial trapping frequency, the system response changes accordingly.

The spring constant in a harmonic potential is given by $\mathbf{F} = -k\mathbf{x}$ with $k = m\omega_{\text{ax}}^2$. Changing k -values have to be compensated with the total PI gain G_{PI} acting as a multiplication factor on \mathbf{F} : $G_{\text{PI}} \propto k \propto \omega_{\text{ax}}^2$. With the relation $\omega_{\text{ax}} \propto \sqrt{V_{\text{ax}}}$ the gain is given by $G_{\text{PI}} \propto V_{\text{ax}} = V_{\text{L1/R1}} - V_{\text{M}}$. By multiplying this total gain with the PI-values from Eq. (2), the ion positioning is achieved for altering axial trapping frequencies. When the potential is deformed, the inter-ion distance increases. If the Coulomb repulsion energy exceeds the potential depth, then ions are leaving the trap, and the desired number of ions is kept in the crystal. In the experiment, we find an ion–ion distance of $60(1) \mu\text{m}$ just before only one ion is kept in the potential. The Coulomb energy reads as $E_{\text{Coul}} = \frac{1}{2}(e^2/4\pi\epsilon_0)(1/d)$, which corresponds to a potential depth $\Phi = E/e$ of $25(1) \mu\text{V}$. The loss of an ion can be detected either by a reduction of the fluorescence light on the EMCCD camera or by a sudden jump of the position of the remaining ion(s). Thus, we may even detect a nonfluorescing ion leaving the potential, making this method applicable to ion crystals consisting of mixed ion species.

To show the high degree of automation, the separation algorithm has been repeated many times; see Fig. 7. Both the general shape of the voltage ramps and the control electrode voltages at the point when the ion crystal is split differ only slightly, here about 10 mV, from shot to shot.

We reach a success probability of 95% for the asymmetric splitting process. We have also realized the symmetric splitting of ion crystals that were positioned above segment M by starting with control voltages of 5, -2, -5, -2, and 5 V for segment L2 to segment R2. When the potential depth is reduced by changing V_{M} , the regulation of V_{L1} guarantees that the center of mass is not changed.

7. CONCLUSION AND OUTLOOK

We have presented an experimental realization of self-adapting and self-regulating algorithms for the automation of fundamental transport routines in a segmented

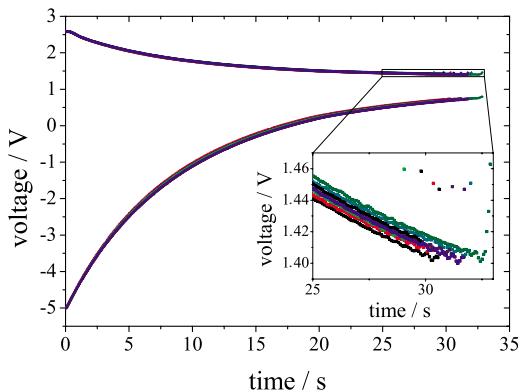


Fig. 7. (Color online) Voltage alterations during repeated splitting experiments. The potential shape is manipulated with segment M (bottom curve), whereas segment L1 (upper curve) regulates the position of the ion. Each splitting cycle is plotted with different colors. The insert shows an enlargement of the control voltage alteration at the very end of the separation process. To keep the remaining ion after separation at the current position, the voltage on segment L1 is abruptly increased.

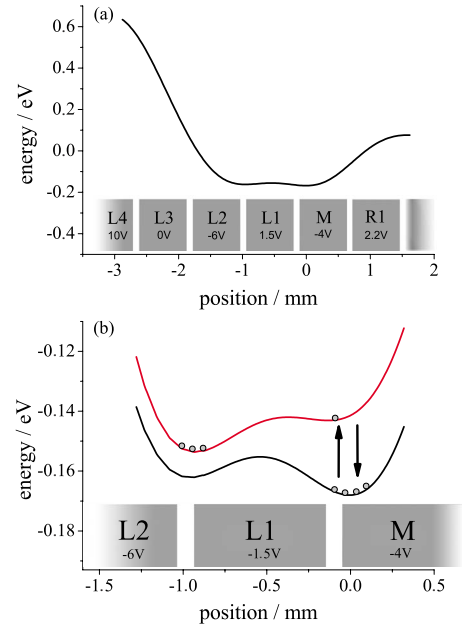


Fig. 8. (Color online) Potentials during the asymmetric separation and reunification process: (a) Axial potential showing a moving minimum above the insulator between segment L1 and L2 and a stationary minimum above the insulator between segment L1 and M. The potential barrier on the left above segments L3 and L4 prevents the ions from leaving the trap during the separation. The voltage configuration displays the situation in the beginning of the separation process. (b) Enlargement of the axial potential showing potentials at the beginning (lower curve), during the separation (upper curve) and for the reunification of the ion crystal (again lower curve). The voltages on the electrodes represent the situation for the potential in the beginning and the reunification of the ion crystal. For clarity, the upper potential has been offset.

linear Paul trap, which are important for quantum information processing with trapped ions. A sensitive camera for the ion detection and a software control of each trap segment is used for building a feedback loop. We show the feedback controlled positioning of an ion to specific locations in the axial direction of the trap via a software PI regulator. By creating two trapping potentials in the axial direction we have shown the separation of ion strings. We have also realized the merging of ion strings after separation into two distinct potentials (see Fig. 8).

These processes can also be performed without the assistance of the camera. For that, the system has to learn the right voltage alterations. Therefore one successful separation process has to be accomplished during which the voltage alterations for the segments are recorded. Higher separation velocities can be achieved by replaying the learned voltage sequence with higher speed without live feedback. The speed-up limit is reached for time scales approaching the axial trap frequency when nonadiabatic effects occur [25]. These effects can be minimized by introducing additional constraints. As an example, the trap frequency could be maintained at a constant value during the transport to avoid parametric heating.

For the future, we envision several improvements of our method: the detection and the overall control loop can be sped up when we use a faster EMCCD camera or only read out a subsection of the image. In our trap, a segment width of $700 \mu\text{m}$ dictates large ion–ion distances, and

therefore low trap frequencies when the splitting occurs. Thus, a major increase in speed is expected when we will apply the method to ion crystals that are stored in a segmented micro-ion-trap with segment dimensions as small as $125\ \mu\text{m}$ [4], where the trap control segments are optimized for ion transport and splitting operations. Another improvement will be a more sophisticated feedback loop. An optimized gradient search may be helpful, especially when not only a single but multiple trap control parameters need to be adapted. Finally, we intend to apply feedback methods not only to the position of the ion crystals, but also to the internal electronic qubit states.

ACKNOWLEDGMENTS

We acknowledge financial support by the Landesstiftung Baden-Württemberg in the framework of the excellence program, the European Commission EMALI (contract MRTN-CT-2006-035369) and STREP MICROTRAP (contract FP6-IST-517675) and the BMBF (06UL264I). We thank W. Schnitzler for proofreading and R. Maiwald for important contributions at an earlier stage of the experiment.

REFERENCES

1. H. Häffner, W. Hänsel, C. F. Roos, J. Benhelm, D. Chekalkar, M. Chwalla, T. Körber, U. D. Rapol, M. Riebe, P. O. Schmidt, C. Becher, O. Gühne, W. Dür, and R. Blatt, "Scalable multi-particle entanglement of trapped ions," *Nature* **438**, 643–646 (2005).
2. R. Blatt and D. J. Wineland, "Entangled states of trapped atomic ions," *Nature* **453**, 1008–1015 (2008).
3. H. Häffner, C. Roos, and R. Blatt, "Quantum computing with trapped ions," *Phys. Rep.* **469**, 155–203 (2008).
4. S. A. Schulz, U. Poschinger, F. Ziesel, and F. Schmidt-Kaler, "Sideband cooling and coherent dynamics in a microchip multi-segmented ion trap," *New J. Phys.* **10**, 045007 (2008).
5. M. A. Rowe, A. Ben-Kish, B. DeMarco, D. Leibfried, V. Meyer, J. Beall, J. Britton, J. Hughes, W. M. Itano, B. Jenlenkovic, C. Langer, T. Rosenband, and D. J. Wineland, "Transport of quantum states and separation of ions in a dual rf ion trap," *Quantum Inf. Comput.* **2**, No. 4, 257–271 (2002).
6. R. B. Blakestad, C. Ospelkaus, A. P. VanDevender, J. M. Amini, J. Britton, D. Leibfried, and D. J. Wineland, "High fidelity transport of trapped-ion qubits through an X-junction trap array," *Phys. Rev. Lett.* **102**, 153002 (2009).
7. G. Huber, T. Deuschle, W. Schnitzler, R. Reichle, K. Singer, and F. Schmidt-Kaler, "Transport of ions in a segmented linear Paul trap in printed-circuit-board technology," *New J. Phys.* **10**, 013004 (2008).
8. R. Reichle, D. Leibfried, R. B. Blakestad, J. Britton, J. D. Jost, E. Knill, C. Langer, R. Ozeri, S. Seidelin, and D. J. Wineland, "Transport dynamics of single ions in segmented microstructured Paul trap arrays," *Fortschr. Phys.* **54**, 666–685 (2006).
9. S. Kuhr, W. Alt, D. Schrader, M. Müller, V. Gomer, and D. Meschede, "Deterministic delivery of a single atom," *Science* **293**, 278–280 (2001).
10. A. Gaëtan, Y. Miroshnychenko, T. Wilk, A. Chotia, M. Vitteau, D. Comparat, P. Pillet, A. Browaeys, and P. Grangier, "Observation of collective excitation of two individual atoms in the Rydberg blockade regime," *Nat. Phys.* **5**, 115–118 (2009).
11. P. Bushev, D. Rotter, A. Wilson, F. Dubin, C. Becher, J. Eschner, R. Blatt, V. Steixner, P. Rabl, and P. Zoller, "Feedback cooling of a single trapped ion," *Phys. Rev. Lett.* **96**, 043003 (2006).
12. J. Chiaverini, D. Leibfried, T. Schaetz, M. D. Barrett, R. B. Blakestad, J. Britton, W. M. Itano, J. D. Jost, E. Knill, C. Langer, R. Ozeri, and D. J. Wineland, "Realization of quantum error correction," *Nature* **432**, 602–605 (2004).
13. M. D. Barrett, J. Chiaverini, T. Schaetz, J. Britton, W. M. Itano, J. D. Jost, E. Knill, C. Langer, D. Leibfried, R. Ozeri, and D. J. Wineland, "Realization of quantum teleportation of atomic qubits," *Nature* **429**, 737–739 (2004).
14. M. Riebe, H. Häffner, C. F. Roos, W. Hänsel, J. Benhelm, G. P. T. Lancaster, T. W. Körber, C. Becher, F. Schmidt-Kaler, D. F. V. James, and R. Blatt, "Deterministic quantum teleportation with atoms," *Nature* **429**, 734–737 (2004).
15. W. Neuhauser, M. Hohenstatt, P. E. Toschek, and H. Dehmelt, "Localized visible Ba⁺ mono-ion oscillator," *Phys. Rev. Lett.* **22**, 1137–1140 (1980).
16. Z. Hu and H. J. Kimble, "Observation of a single atom in a magneto-optical trap," *Opt. Lett.* **19**, 1888–1890 (1994).
17. D. Haubrich, H. Schadwinkel, F. Strauch, B. Ueberholz, R. Wynands, and D. Meschede, "Observation of individual neutral atoms in magnetic and magneto-optical traps," *Europhys. Lett.* **34**, 663–668 (1996).
18. N. Schlosser, G. Reymond, I. Protsenko, and P. Grangier, "Sub-poissonian loading of single atoms in a microscopic dipole trap," *Nature* **411**, 1024–1027 (2001).
19. Material P97, Isola AG, Germany.
20. DAC8814, Texas Instruments.
21. S. Gulde, D. Rotter, P. Barton, F. Schmidt-Kaler, R. Blatt, and W. Hogervorst, "Simple and efficient photoionization loading of ions for precision ion-trapping experiments," *Appl. Phys. B* **73**, 861–863 (2001).
22. Andor iXon DV885.
23. D. F. V. James, "Quantum dynamics of cold trapped ions with application to quantum computation," *Appl. Phys. B* **66**, 181–190 (1998).
24. K. Singer, U. Poschinger, M. Murphy, P. Ivanov, F. Ziesel, T. Calarco, and F. Schmidt-Kaler, "Colloquium: experiments with atomic quantum bits—essential numerical tools," arXiv.org, arXiv:0912.0196 (2009).
25. S. Schulz, U. Poschinger, K. Singer, and F. Schmidt-Kaler, "Optimization of segmented linear Paul traps and transport of stored particles," *Fortschr. Phys.* **54**, 648–665 (2006).